AMERICAN SOCIETY FOR MICROBIOLOGY | **Infection and Immunity**®

Vacuolation Activity and Intracellular Trafficking of ArtB, the Binding Subunit of an AB5 Toxin Produced by *Salmonella enterica* Serovar Typhi

Brock P. Herdman,[a] James C. Paton,[a] Hui Wang,[a] Travis Beddoe,[b]
Adrienne W. Paton[a]

Research Centre for Infectious Diseases, Department of Molecular and Cellular Biology, University of Adelaide, Adelaide, SA, Australia[a]; Department of Animal, Plant and Soil Science, Centre for AgriBiosciences, La Trobe University, Bundoora, Victoria, Australia[b]

ABSTRACT Various *Salmonella enterica* serovars, including *S. enterica* serovar Typhi, encode an AB5 toxin (ArtAB), the A subunit of which is an ADP-ribosyltransferase related to the S1 subunit of pertussis toxin. However, although the A subunit is able to catalyze ADP-ribosylation of host G proteins, a cytotoxic phenotype has yet to be identified for the holotoxin. Here we show that its B subunit pentamer (ArtB) binds to receptors on the surface of Vero (African green monkey kidney) cell, CHO (Chinese hamster ovary) cell, U937 (human monocyte) cell, and HBMEC (human brain microvascular endothelial cell) lines. Moreover, ArtB induced marked vacuolation in all cell lines after 4 h of incubation. Further studies in Vero cells showed that vacuolation was inhibited by bafilomycin A1 and was dependent on the clathrin-mediated uptake of ArtB. Vacuolation was also inhibited by treatment of cells with neuraminidase, indicating that sialylated glycans are functional receptors for ArtB. Confocal colocalization studies indicated that after cell binding and internalization, ArtB undergoes retrograde transport via early endosomes, the *trans*-Golgi network, and the Golgi apparatus, reaching the endoplasmic reticulum (ER) after approximately 2 h. The onset of vacuolation also coincided with gross cytoskeletal reorganization. At later time points, ArtB colocalized with ER-Tracker Red in the vacuolar membrane, implying that vacuolation is a consequence of ER disorganization. Thus, the isolated B subunit of this cryptic AB5 toxin has significant effects on target cells with the potential to contribute directly to pathogenesis independently of the catalytic A subunit.

KEYWORDS AB5 toxins, B subunit, *Salmonella*, vacuolation

AB5 toxins are critical weapons in the armory of virulence factors deployed by several major bacterial pathogens. They comprise a catalytic A subunit noncovalently linked to a pentameric B subunit. Their mechanism of action commences with the binding of the B subunit pentamer to specific glycan receptors on the cell surface, triggering the uptake of the holotoxin. The A subunit is then able to covalently modify intracellular substrates, inhibiting or corrupting essential host functions (1). The AB5 toxins characterized to date are classified into four families according to A subunit sequence homology and catalytic activity as well as the structural organization of the holotoxin (1). The A subunits of both the cholera toxin (Ctx) and pertussis toxin (Ptx) families are ADP-ribosyltransferases that respectively modify $G_s\alpha$ and $G_i\alpha$ proteins in the host cell cytosol, disrupting their signal transduction pathways. The A subunits of the Shiga toxin (Stx) family are RNA *N*-glycosidases that cleave a specific adenine base from 28S rRNA, inhibiting eukaryotic protein synthesis. The fourth and most recently discovered AB5 toxin family is *Escherichia coli* subtilase cytotoxin (SubAB), produced by a subset of strains that also produce Stx (2). Its A subunit

is a highly specific subtilase-like serine protease that cleaves the essential endoplasmic reticulum (ER) chaperone BiP/GRP78, thereby inducing a massive ER stress response and triggering cellular apoptosis (3–6).

The B subunits of the Ctx and Stx families are homopentamers that recognize glycans displayed by host gangliosides and glycosphingolipids, respectively (1). In contrast, the B subunit of Ptx comprises 4 nonidentical subunits (subunits S2, S3, S4, and S5) in a 1:1:2:1 stoichiometry. The S2 and S3 subunits of Ptx bind to sialylated glycoproteins rather than glycolipids (1). The B subunit of SubAB (SubB) is a homopentamer that exhibits a strong specificity for glycans terminating in α2-3-linked N-glycolylneuraminic acid (Neu5Gc). In spite of relatively low amino acid sequence identity, SubB and the C-terminal portion of the Ptx S2 subunit exhibit strong structural homology (7). As is the case for the Ptx S2 and S3 subunits, the glycan binding pockets on SubB are located on the sides of the pentamer, consistent with an interaction with cell surface glycoproteins. In contrast, the glycan binding pockets of CtxB and StxB are located on the base, close to the membrane, enabling interactions with glycolipids (7).

Homologues of SubB are encoded on the genomes of both *Yersinia pestis* (57% amino acid identity) and *Salmonella enterica* serovar Typhi (51% identity) (2) as well as in other yersiniae and *S. enterica* serovars, including *S. enterica* serovars Paratyphi, Typhimurium, Montevideo, and Arizonae. These proteins have now been classified as superfamily PRK15265 ("subtilase cytotoxin B subunit-like proteins"). In *Salmonella*, but not in *Yersinia*, the genes are cotranscribed with homologues of the Ptx catalytic S1 subunit. The putative *S*. Typhimurium AB5 toxin has been named ArtAB (ADP-ribosylating toxin) (8), and like Ptx S1, *S*. Typhimurium ArtA is an ADP-ribosyltransferase capable of modifying host cell G proteins (9). Although no ADP-ribosyltransferase-dependent cytotoxic phenotype has been identified for ArtAB, the homologue from *S*. Typhi (also referred to as PltAB [for pertussis-like toxin]) has been reported to associate with cytolethal distending toxin (CdtB) and deliver it from an intracellular compartment to target cells via autocrine and paracrine pathways (10). Both the A and B subunits were required for this property, but it was not dependent on ADP-ribosyltransferase activity (10). Structural analysis indicated that the CdtB-PltA interaction is stabilized by a disulfide bond, resulting in a unique A2:B5 overall toxin configuration, but the critical Cys residue in PltA is not present in homologues (ArtA) found in other salmonellae (11).

Apart from mediating the internalization of holotoxin, the interaction of AB5 toxin B subunits with receptors on the surface of target cells has the potential to impact a variety of signaling pathways. Thus, the B subunits may directly contribute to pathogenesis by triggering host responses independently of their respective catalytic ("toxic") A subunits. Indeed, we have shown that purified *S*. Typhi ArtB elicits cytokine, chemokine, and adhesion molecule responses in human monocyte, colonic epithelial, and brain microvascular endothelial cell lines (12). In the present study, we have investigated the uptake and intracellular trafficking of ArtB and demonstrate its capacity to induce a severe vacuolation phenotype.

RESULTS

Binding of ArtB to cell lines. As an initial experiment, the capacity of purified ArtB labeled with DyLight 488 to bind to various cell lines was investigated by using flow cytometry (Fig. 1). Cells were incubated for 60 min with 10 μg/ml ArtB at 4°C to prevent internalization. There was strong labeling of Vero, U937, and CHO cells under these conditions, as judged by mean fluorescence intensity, with somewhat weaker labeling of human brain microvascular endothelial cells (HBMECs).

Vacuolation activity of ArtB. Vero cells, U937 cells, and HBMECs were examined by phase-contrast microscopy after treatment with ArtB for up to 24 h (Fig. 2). A pronounced vacuolation phenotype was apparent in all cell lines from 4 h and was dramatic at 24 h. Similar results were obtained for CHO cells (data not shown). When vacuolation was compared in Vero cells treated with 10 μg/ml ArtB and those treated with 13.25 μg/ml ArtAB holotoxin (equimolar doses with respect to the B subunit), there was no apparent difference in phenotype after 1, 4, or 24 h (Fig. 3). Binding to
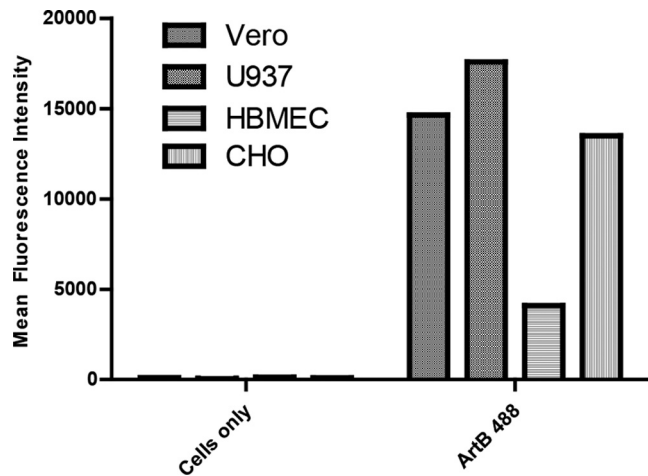
FIG 1 Binding of ArtB to cells. Vero cells, U937 cells, HBMECs, and CHO cells were incubated with or without DyLight 488-labeled ArtB (10 μg/ml) for 60 min at 4°C and examined by flow cytometry, as described in Materials and Methods. Data are mean fluorescence intensities derived from 10,000 cell counts; data are representative of results from two independent experiments.

U937 cells was also compared by fluorescence-activated cell sorter (FACS) analysis, using unlabeled ArtB and ArtAB at the same doses. No difference in mean fluorescence intensity was detected after staining with monoclonal anti-His$_6$ (Roche) followed by Alexa 488-labeled secondary antibody (result not shown). Thus, the presence of the catalytic A subunit does not significantly impact binding to target cells or B subunit-mediated vacuolation.

The vacuolation phenomenon was then examined quantitatively in Vero cells by measuring the uptake of Neutral Red dye, an acidotrophic, membrane-permeable amine that accumulates in the vacuolar lumen, as shown for ArtB-treated Vero cells in Fig. 4A. Uptake was dose dependent, reaching statistical significance ($P < 0.05$) at 1 μg/ml, and was maximal at 5 to 10 μg/ml ($P < 0.001$) after 4 h of incubation (Fig. 4B). Extending the incubation time to 24 h reduced the detection threshold further to 0.5 μg/ml (Fig. 4D). At a dose of 10 μg/ml, ArtB-induced Neutral Red uptake steadily increased over the 4-h incubation period and reached statistical significance relative to the untreated control cells by 1 h ($P < 0.001$) (Fig. 4C). Neutral Red uptake was also measured in Vero cells that had been exposed to 1 to 10 μg/ml ArtB for limited time periods, followed by the removal of exogenous ArtB by washing the cells and replacement of the culture medium for the remainder of the 4-h incubation period (Fig. 5). At the highest dose, exposure for as little as 5 min was sufficient to elicit significant dye uptake, and 15 min of exposure resulted in levels of vacuolation indistinguishable from those in cells treated continuously with ArtB for 4 h. However, at lower doses, more prolonged exposures to ArtB were required.

Effect of inhibitors on vacuolation. The Neutral Red uptake assay was also used to assess the impact of a range of inhibitors of cellular processes on vacuolation induced by treatment with 10 μg/ml ArtB for 4 h (Fig. 6). Dye uptake was completely inhibited (absorbance at 540 nm [A_{540}] value less than or equal to that of non-ArtB-treated control cells) in K$^+$-depleted medium or medium with hypertonic (450 mM) sucrose, conditions which inhibit the formation of clathrin-coated pits (13, 14). Similarly, a complete blockade of Neutral Red uptake was achieved by treatment with 16 μg/ml chlorpromazine or 50 μM monodansylcadaverine (MDC), both of which also specifically inhibit clathrin-mediated endocytosis (14, 15) (Fig. 6). Thus, vacuolation appears to be dependent on the clathrin-mediated internalization of ArtB. Vacuolation was also significantly inhibited by treatment with as little as 10 nM bafilomycin A1, which inhibits the vacuolar-type H$^+$-ATPase (V-ATPase) (16) (Fig. 5).

In contrast, Neutral Red uptake was only slightly, albeit significantly ($P < 0.05$), reduced by treatment with 200 μM genistein, a tyrosine kinase inhibitor that blocks
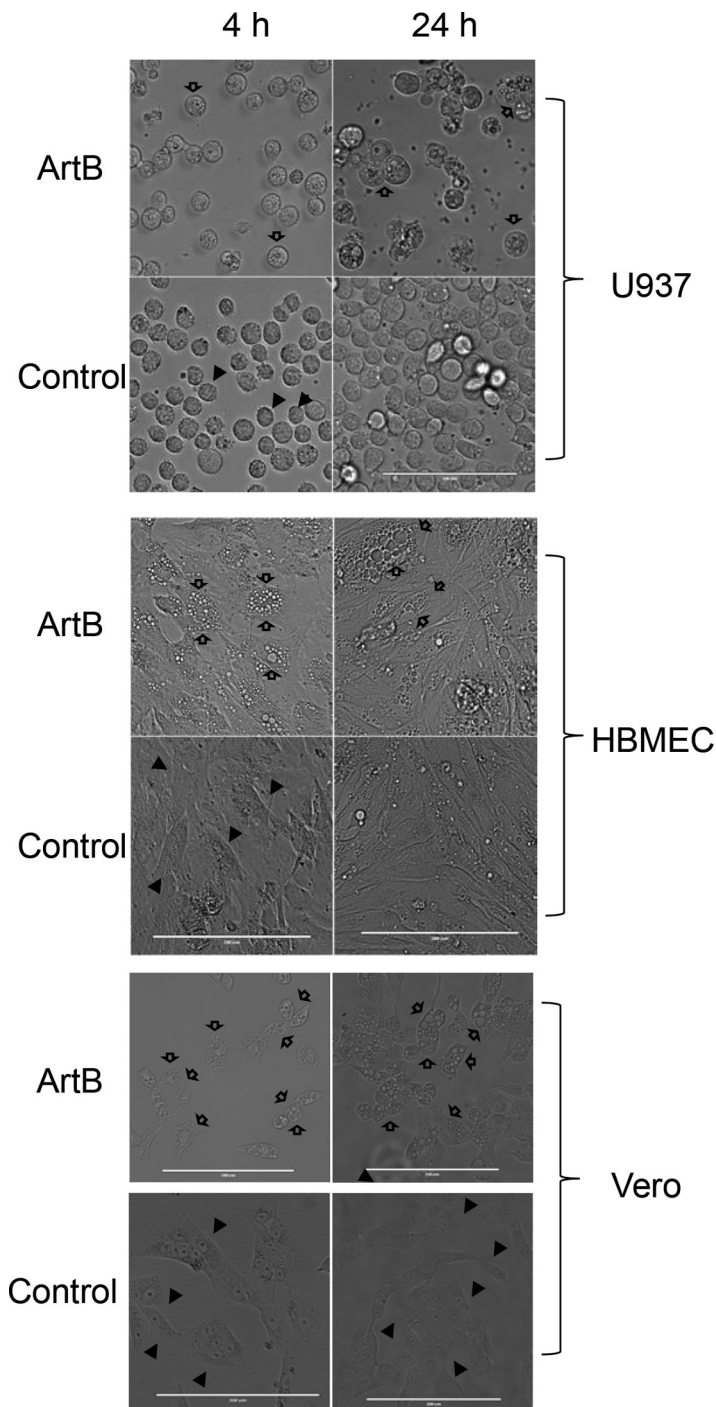
FIG 2 Induction of cellular vacuolation by ArtB. U937 cells, HBMECs, and Vero cells were incubated with or without 10 μg/ml ArtB for 4 or 24 h, as indicated, and then examined by phase-contrast microscopy (bars = 0.1 mm [top {U937}] and 0.2 mm [middle and bottom]). Solid arrows, normal cells; hollow arrows, vacuolated cells.

endocytosis via caveolae and lipid rafts (17, 18), while 20 μM nystatin, which also blocks caveolar endocytosis (19), had no significant inhibitory effect (Fig. 6). On the other hand, treatment with 100 μM dynasore, a GTPase inhibitor that targets dynamin-mediated endocytosis, reduced uptake by approximately two-thirds (Fig. 6). Neutral Red uptake was not significantly reduced by treatment with 10 μg/ml nocodazole, which binds to tubulin and interferes with microtubule polymerization, but 10 μg/ml
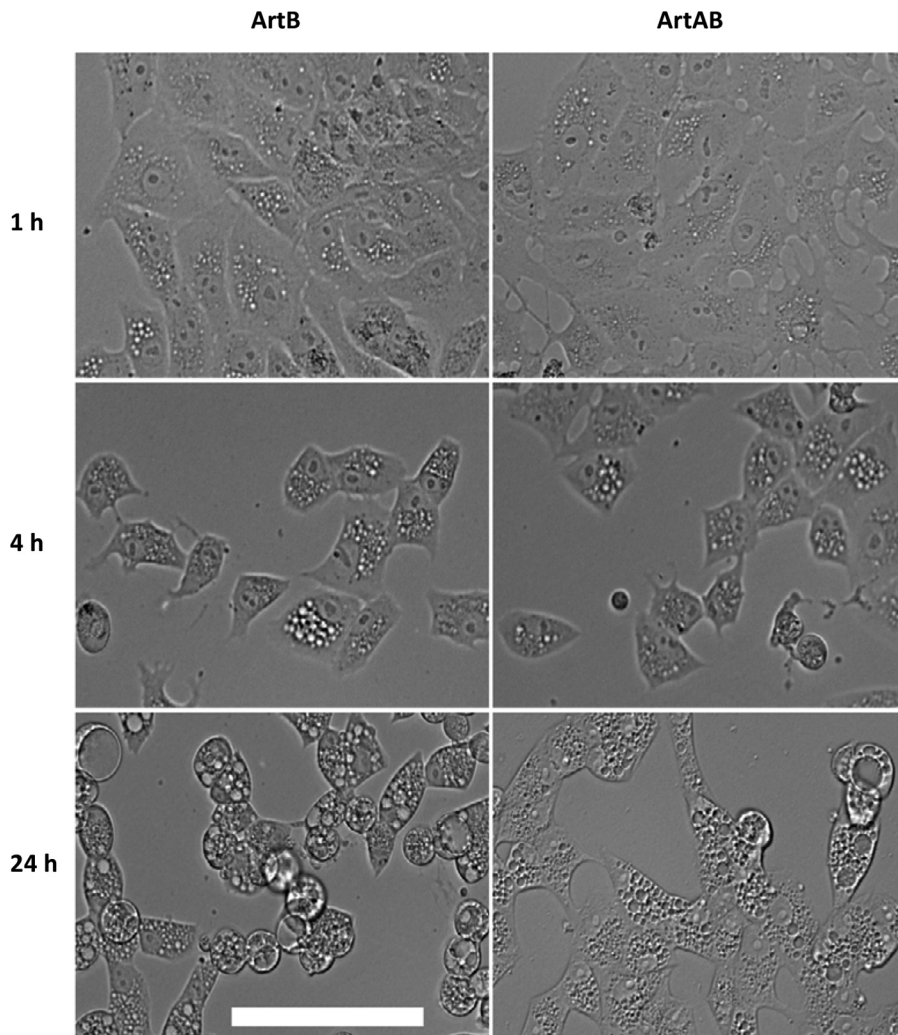
FIG 3 Vacuolation of Vero cells by ArtB or ArtAB. Vero cells were incubated with 10 μg/ml ArtB or 13.25 μg/ml ArtAB (equimolar with respect to ArtB) for 1, 4, or 24 h and then examined by phase-contrast microscopy (bar = 0.1 mm).

brefeldin A, which inhibits protein transport between the Golgi and ER compartments, led to ~30% inhibition. Importantly, Neutral Red uptake was also significantly reduced (by approximately 70%) in cells treated with the neuraminidase NanA (Fig. 6), suggesting that the vacuolation phenotype is dependent on interactions between ArtB and cognate sialylated glycans on the cell surface.

Fluorescence colocalization with subcellular markers. The above-described findings suggest that the uptake of ArtB by Vero cells occurs largely via clathrin-coated vesicles. To further examine intracellular trafficking pathways, the colocalization of ArtB with various subcellular markers was examined by confocal microscopy over a 4-h period. Vero cell monolayers were pulsed with 10 μg/ml ArtB for 30 min, washed twice with phosphate-buffered saline (PBS), and placed into fresh medium for the remainder of the incubation period, prior to fixation and staining (Fig. 7). Significant colocalization was observed with the early endosome marker Rab5, peaking at 2 h (46%, 55%, and 42% colocalization at 1, 2, and 4 h, respectively). Rab5 is a small GTPase localized to early endosomes. It regulates fusion between endocytic vesicles and early endosomes as well as homotypic fusion between early endosomes (20). Significant colocalization was also observed with EEA-1, peaking at 4 h (27%, 38%, and 44% colocalization at 1, 2, and 4 h, respectively). EEA-1 is an early endosomal Rab5 effector protein that has been implicated in the docking of incoming endocytic vesicles before fusion with early
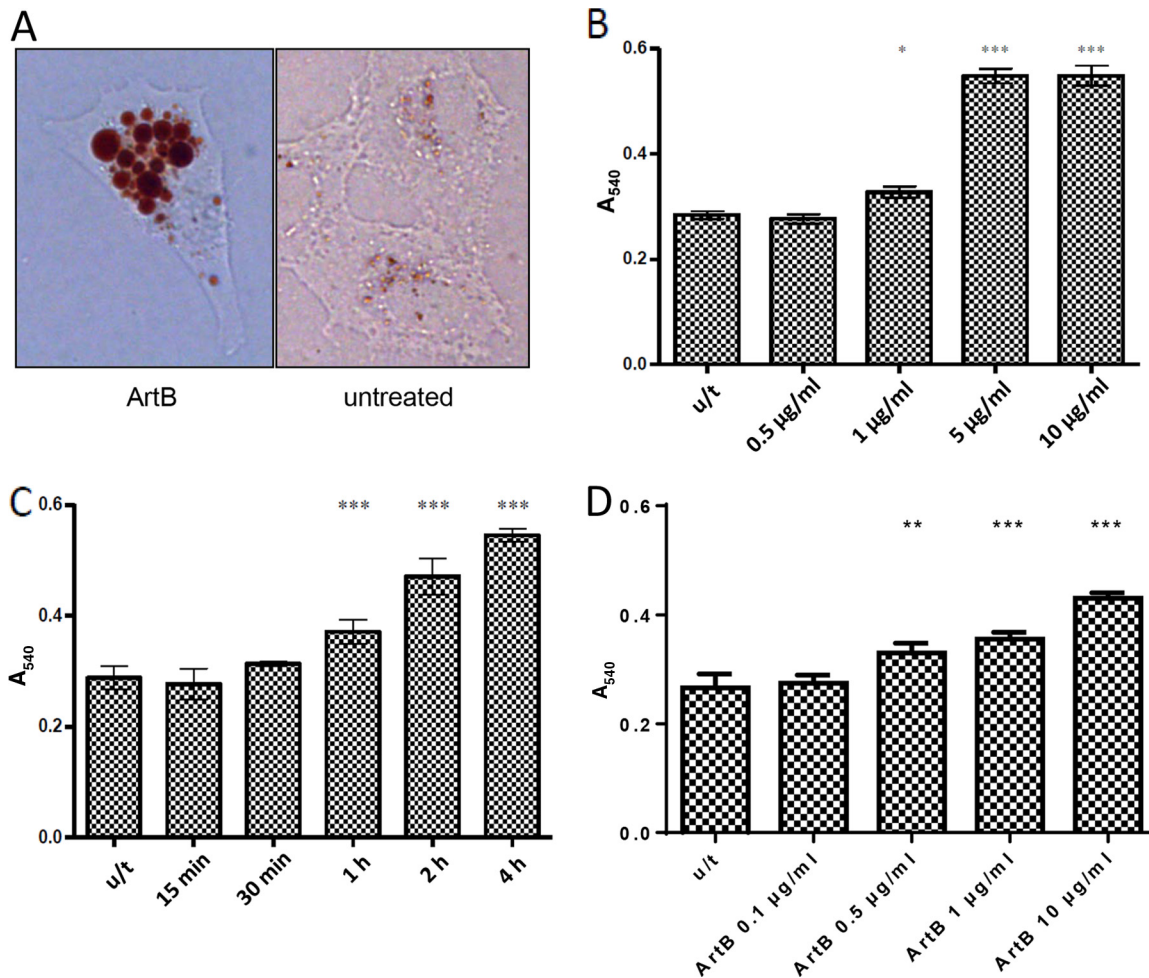
FIG 4 Neutral Red uptake by ArtB-treated Vero cells. (A) Light micrograph showing Neutral Red dye incorporation into vacuoles by Vero cells treated with or without 10 μg/ml ArtB. (B) Dose response. Vero cells were treated with the indicated doses of ArtB for 4 h, and Neutral Red uptake was measured spectrophotometrically, as described in Materials and Methods. (C) Time course. Vero cells were treated with 10 μg/ml ArtB for the indicated times and then assayed for Neutral Red uptake. Data are A_{540} values (means $\pm$ standard errors of the means from at least three experiments). (D) Dose response after 24 h of incubation. *, $P < 0.05$; **, $P < 0.01$; ***, $P < 0.001$ (relative to untreated [u/t] control cells, as determined by Student's unpaired, two-tailed t test).

endosomes (21). Colocalization with Rab9, a late endosome marker involved in vesicle transport to the *trans*-Golgi network (TGN) (22), was also observed, and this was maximal at 4 h (40%, 52%, and 65% colocalization at 1, 2, and 4 h, respectively). A lesser degree of colocalization, which did not increase with time (32%, 32%, and 34% colocalization at 1, 2, and 4 h, respectively), was observed with Rab7, which is expressed in late endosomes targeted to the lysosome (23). Colocalization with wheat germ agglutinin (WGA), which binds to target glycans expressed in the Golgi apparatus, was more evident at 4 h than at earlier time points (20%, 22%, and 32% colocalization at 1, 2, and 4 h, respectively). Similarly, the colocalization of ArtB with the *trans*-Golgi network protein golgin 97 was more evident at 4 h than at earlier time points (11%, 12%, and 22% colocalization at 1, 2, and 4 h, respectively). The colocalization of ArtB with ER-Tracker Red (ER-TR) increased steadily during the 4-h incubation period (37%, 68%, and 72% colocalization at 1, 2, and 4 h, respectively) (Fig. 7).

Interestingly, staining of DyLight 488-labeled ArtB-treated cells with Alexa Flour 594-phalloidin, which labels F-actin, showed a progressive disorganization of the cytoskeleton at between 30 min and 4 h (Fig. 8). Colocalization studies were also conducted by using Vero cells treated with DyLight 488-labeled ArtB for 16 h, by which time vacuolation was extensive. ArtB and ER-Tracker Red showed strong colocalization in the vacuolar membrane, suggesting that the vacuoles are derived from the ER
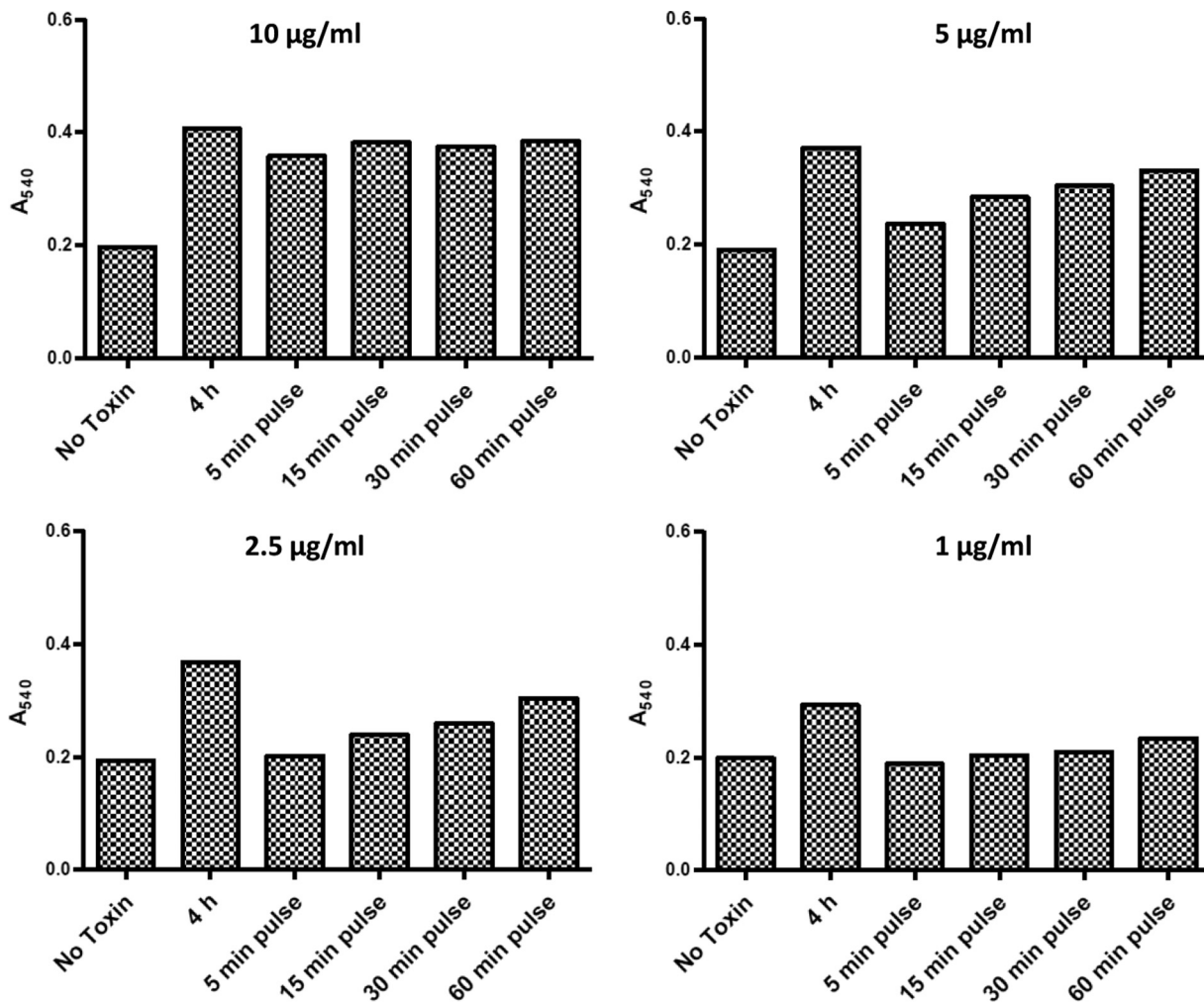
FIG 5 Neutral Red uptake by Vero cells after short-term exposure to ArtB. Vero cells were incubated with various doses of ArtB, and after the indicated times, monolayers were washed, the medium was replaced, and incubation was continued for up to a total of 4 h. Neutral Red dye uptake (A_{540}) was then assayed as described in the text.

(Fig. 9). In contrast, there was no significant colocalization with LysoTracker Red or MitoTracker Red at either 16 h (Fig. 9) or earlier time points (not shown).

We also explored the link between vacuolation, ArtB trafficking, and cytoskeletal rearrangements. Pretreatment with bafilomycin A1 to block vacuolation did not have a significant effect on the uptake and trafficking of ArtB to the ER (Fig. 10). However, bafilomycin A1 appeared to prevent cytoskeletal rearrangements, indicated by F-actin staining (Fig. 11). Thus, there appears to be a direct link between vacuolation and F-actin distribution.

DISCUSSION

In the present study, we have shown that ArtB, the glycan binding B subunit pentamer of a cryptic *S.* Typhi AB5 toxin, induces a strong vacuolating phenotype in a variety of cultured cell lines, notably Vero cells, CHO cells, U937 cells, and HBMECs. Vacuolation was evident by phase-contrast microscopy at 4 h but was far more extensive at 24 h. Nevertheless, a more detailed characterization of the phenomenon in Vero cells revealed significant vacuolation within 1 h of treatment and at ArtB doses as low as 1 μg/ml, as judged by a Neutral Red uptake assay. At high doses, only a brief exposure to ArtB was required to elicit near-maximal vacuolation, as washing of the treated cells after as little as 5 min of incubation did not prevent subsequent vacuole development. This is consistent with the rapid binding and internalization of ArtB, as is
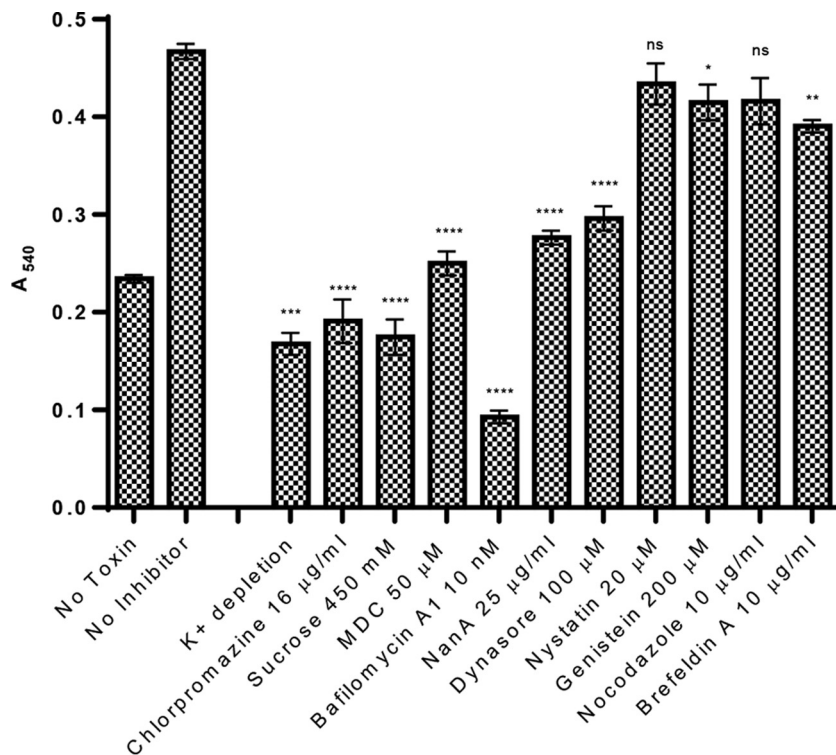
FIG 6 Effects of inhibitors on ArtB-induced Neutral Red uptake. Vero cells were treated with 10 μg/ml ArtB after the depletion of intracellular potassium (see Materials and Methods) or after treatment with various inhibitors at the indicated concentrations and then assayed for Neutral Red uptake. Data are presented as A_{540} values (means $\pm$ standard errors of the means from at least three experiments). *, $P < 0.05$; **, $P < 0.01$; ***, $P < 0.001$; ****, $P < 0.0001$; ns, not significant (relative to cells treated with ArtB without inhibitors, as determined by one-way ANOVA).

known to occur for other AB5 holotoxins (2, 24). Treatment with neuraminidase significantly inhibited vacuolation, indicating that sialylated glycans on the Vero cell surface are functional receptors for ArtB. Both *E. coli* SubB and the S2 subunit of Ptx, which share partial sequence identity with ArtB, also bind specifically to sialylated glycans (those terminating in α2-3-linked Neu5Gc and *N*-acetylneuraminic acid [Neu5Ac], respectively) (1, 7). *S.* Typhi ArtB/PltB was recently shown to have a strong binding specificity for glycans terminating in the consensus sequence Neu5Acα2-3Galβ1-3/β1-4Glc/GlcNAc, with much reduced binding to analogous structures terminating in Neu5Gc (25). Thus, SubB and ArtB appear to exhibit opposite preferences for Neu5Ac- versus Neu5Gc-terminating glycans.

The significant inhibition of ArtB-mediated neutral red uptake by cells grown in K$^+$-depleted medium, or medium with hypertonic sucrose, suggested a requirement for clathrin-mediated endocytosis, and this was confirmed by inhibition with chlorpromazine and MDC. In contrast, treatment with genistein, a tyrosine kinase inhibitor that blocks endocytosis via caveolae and lipid rafts (17, 18), caused only slight albeit significant inhibition, while nystatin had no significant effect at all. The strong dependence of ArtB on clathrin-mediated uptake is a further point of similarity with SubB, although the slight inhibitory effect of genistein is reminiscent of CtxB and StxB, which engage both clathrin-dependent and lipid raft uptake pathways (24). Complete inhibition of ArtB-mediated vacuolation by bafilomycin A1 treatment also indicated a requirement for V-ATPase.

Confocal microscopic colocalization studies during the first 4 h after ArtB treatment showed that following binding to the cell surface, ArtB underwent retrograde transport via early and late endosomes and the Golgi apparatus to the ER. The colocalization of ArtB with Rab5 was maximal at the 2-h time point, while colocalization with EEA-1 was
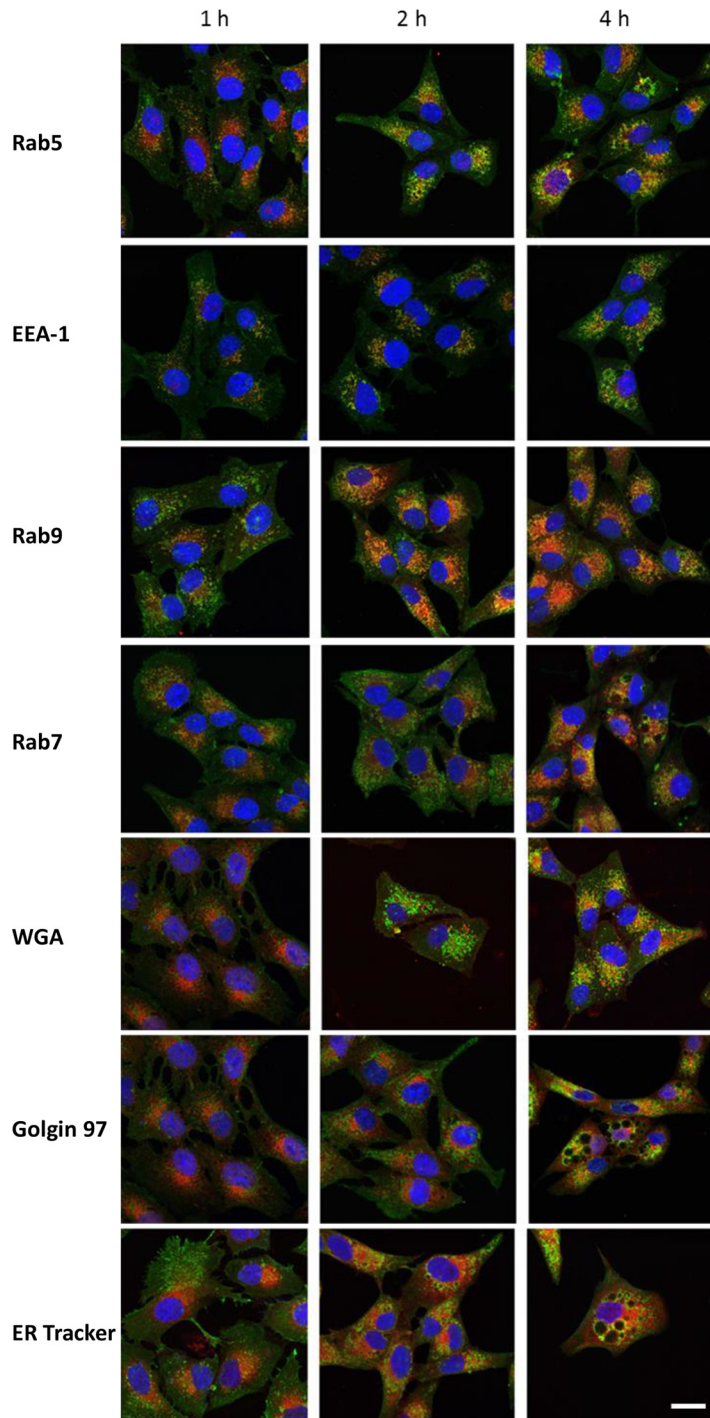
FIG 7 Colocalization of ArtB with Rab5, EEA-1, Rab9, Rab7, WGA, golgin 97, or ER-Tracker Red. Vero cells were pulsed with ArtB (10 μg/ml) for 30 min, washed twice with PBS, and incubated in fresh medium for the remainder of the indicated times. Cells were then fixed, permeabilized, and stained with anti-His$_6$ (to detect ArtB) and either anti-Rab5, -EEA-1, -Rab9, -Rab7, -WGA, -golgin 97, or -ER-Tracker Red, followed by fluorescent secondary antibodies, as appropriate. Cells were then examined by confocal microscopy as described in Materials and Methods. The nuclei were stained with DAPI (bar, 20 μm).

greater at 4 h. Colocalization with Rab9, WGA, and ER-Tracker Red was also maximal at 4 h. In contrast, there was only minimal colocalization of ArtB with Rab7 at any of the time points, indicating that significant amounts of the toxin are not targeted to lysosomes. The intracellular trafficking route followed by ArtB is similar to that we
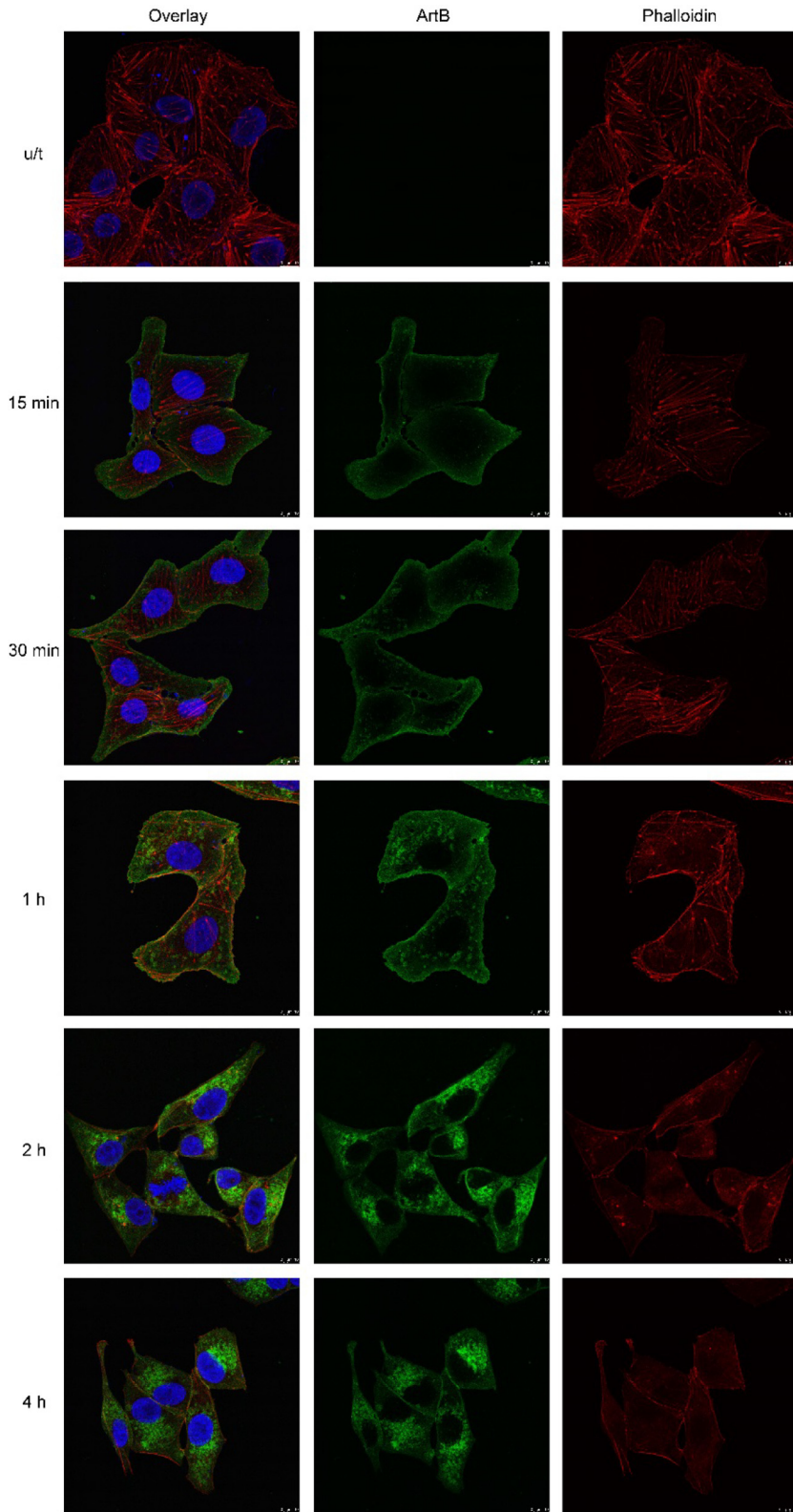
FIG 8 Effect of ArtB on the cytoskeleton. Vero cells were incubated with DyLight 488-labeled ArtB (10 μg/ml) for the indicated times, after which cells were fixed and permeabilized, and F-actin was stained with 5 U/ml Alexa Flour 594-phalloidin and then examined by confocal microscopy, as described in Materials and Methods. Separate ArtB and phalloidin channels are shown, as are overlaid images with nuclei also stained with DAPI.
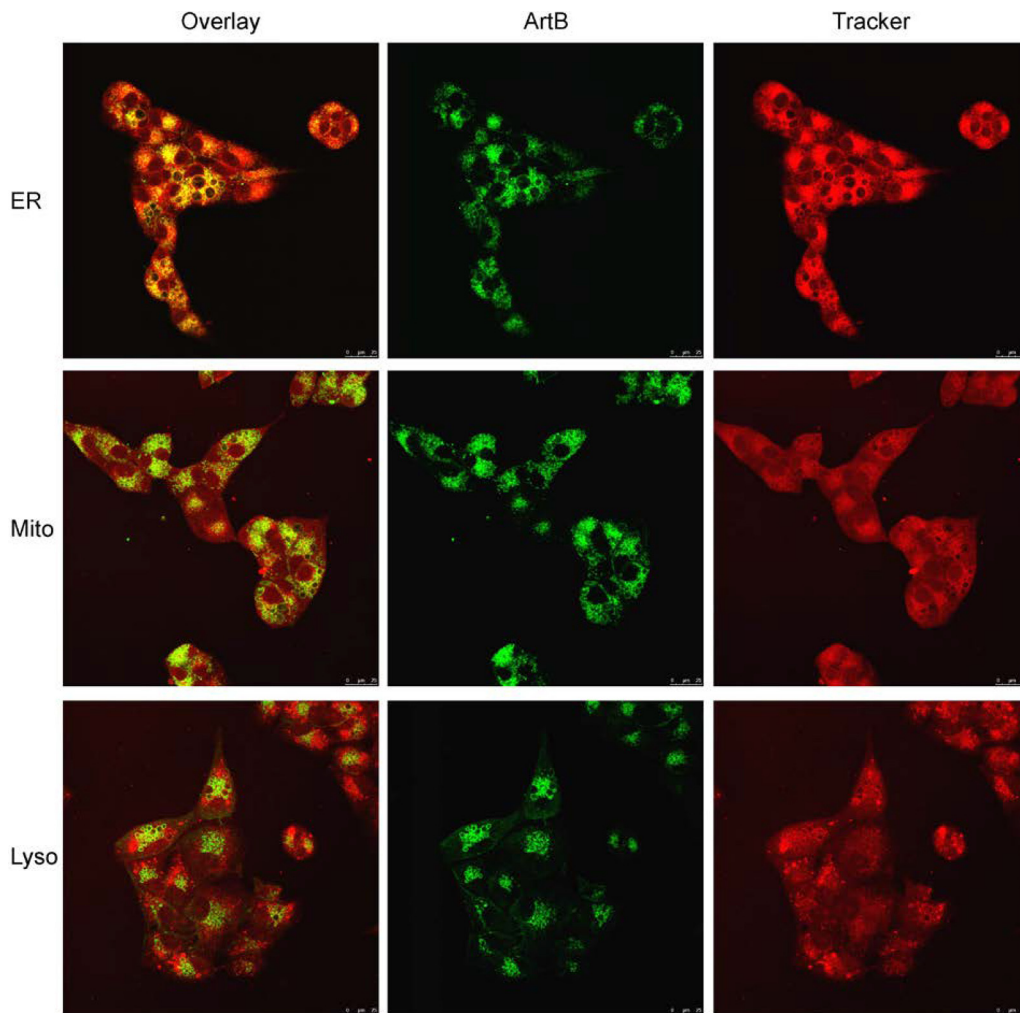
FIG 9 Colocalization of ArtB with ER, mitochondrial, and lysosomal markers at 16 h. Vero cells were incubated with DyLight 488-labeled ArtB (10 μg/ml) for 16 h, with 2.5 μM ER-Tracker Red, 400 nM MitoTracker Red, or 250 nM LysoTracker Red being added for the final 30 min, after which cells were fixed and then examined by confocal microscopy as described in Materials and Methods. Separate ArtB and Tracker channels are shown, as is an overlaid image (nuclei unstained) (bar, 25 μm).

reported previously for SubAB (24), although the speed of trafficking of SubAB was much higher, with detectable levels of toxin arriving in the ER compartment within 30 min. Importantly, treatment with ArtB resulted in the disorganization of the cytoskeleton, as judged by F-actin staining with Alexa Fluor 594-phalloidin, which was clearly evident by as early as 1 h and progressively increased thereafter. At 16 h, by which time vacuolation was profound, there was strong colocalization of ArtB with ER-Tracker Red at the vacuolar membrane, but this was not seen with LysoTracker Red or MitoTracker Red, suggesting that the vacuoles result from the disorganization of the ER compartment. The precise molecular events underlying ArtB-mediated ER disruption and vacuole formation remain to be elucidated. Both vacuolation and cytoskeletal disruption are inhibited by bafilomycin A1, indicating a dependence on the V-ATPase. In contrast, bafilomycin A1 had no effect on the uptake of ArtB or retrograde trafficking to the ER, indicating that intracellular trafficking and vacuolation are independent processes.

Several other bacterial toxins have been reported to form vacuoles in eukaryotic cells, most notably VacA produced by *Helicobacter pylori*. VacA is secreted by *H. pylori* as an 88-kDa species, which is subsequently cleaved into 33-kDa and 55-kDa N- and C-terminal domains that remain associated, like typical A-B toxins. Although VacA lacks enzymatic activity, the toxin forms hexameric anion-selective pores in target membranes (26). After binding, VacA is internalized by a lipid raft-dependent, clathrin-
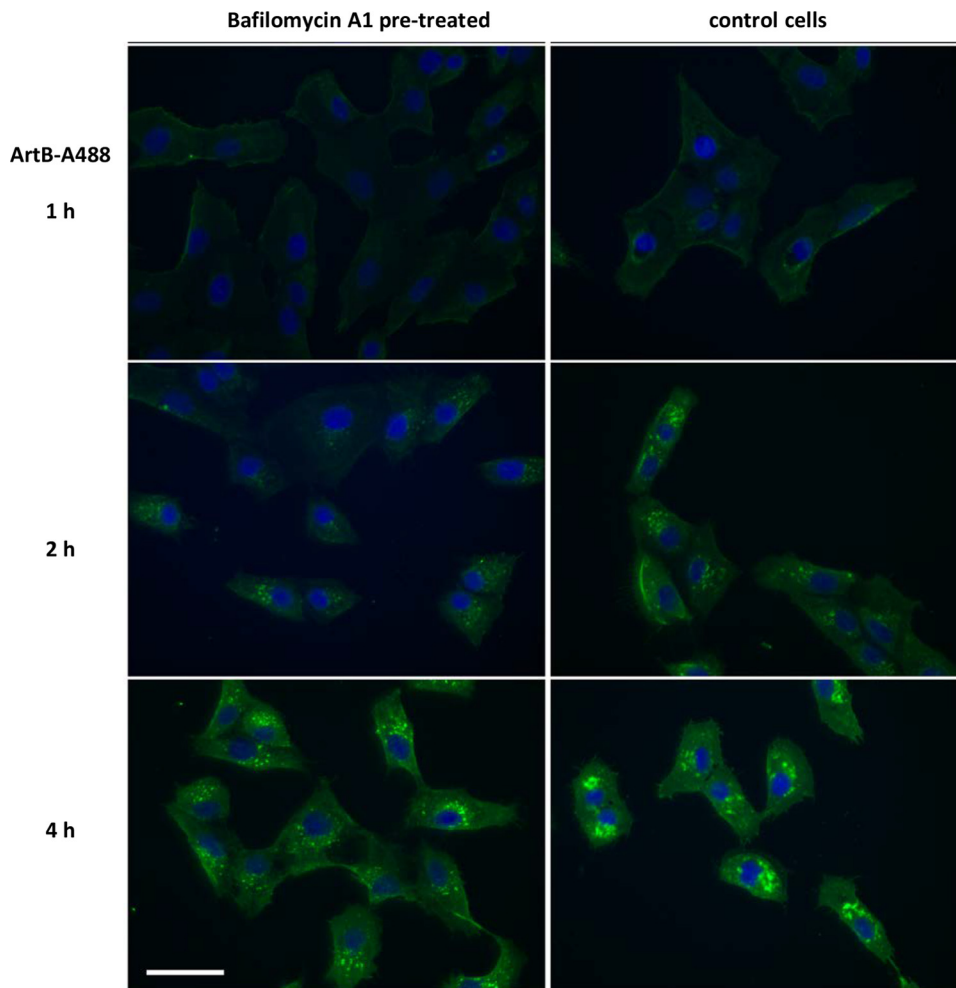
FIG 10 Effect of bafilomycin A1 on ArtB cell binding/intracellular trafficking. Vero cells were pretreated with bafilomycin A1 (10 nM) for 1 h or left untreated (control cells) and then incubated with DyLight 488-labeled ArtB (ArtB-A488) for the indicated times, after which cells were fixed and examined by using an EVOS-fl high-resolution digital inverted fluorescence microscope. Bar, 50 μm.

independent process into endosomes that are targeted to the mitochondria in an F-actin-dependent process, eventually triggering apoptosis (26). However, during this intracellular journey, the presence of VacA pores causes osmotic swelling of the endosomes, resulting in vacuolation. *Clostridium perfringens* epsilon-toxin is another example of a pore-forming toxin that is taken up via the lipid raft pathway and then trafficked via early endosomes, ultimately forming vacuoles derived from late endosomes and lysosomes, as judged by the colocalization of the toxin with Rab7 and lysosome-associated membrane protein 2 (LAMP2) (27). Thus, there are marked differences in the modes of uptake and the intracellular trafficking pathways of VacA, epsilon-toxin, and ArtB. *Mycoplasma pneumoniae* community-acquired respiratory distress syndrome (CARDS) toxin is another example of an A-B toxin capable of vacuolating cells. Like ArtB, it is internalized by clathrin-mediated endocytosis, but the vacuole membranes are enriched in Rab9, LAMP1, and LAMP2, suggesting an endosomal/lysosomal origin (28–30). A further distinction between ArtB and CARDS toxin is that the latter has ADP-ribosyltransferase activity, and mutagenesis of a critical enzyme active-site amino acid almost completely abolishes vacuolating activity (29). Coincidentally, ArtA, the cognate A subunit of ArtB, is also an ADP-ribosyltransferase capable of modifying host cell G proteins (9), but to date, no cytopathic phenotype has been associated with the enzymatic activity of the AB5 holotoxin.

From the data described above, it is clear that the mechanisms by which vacuoles
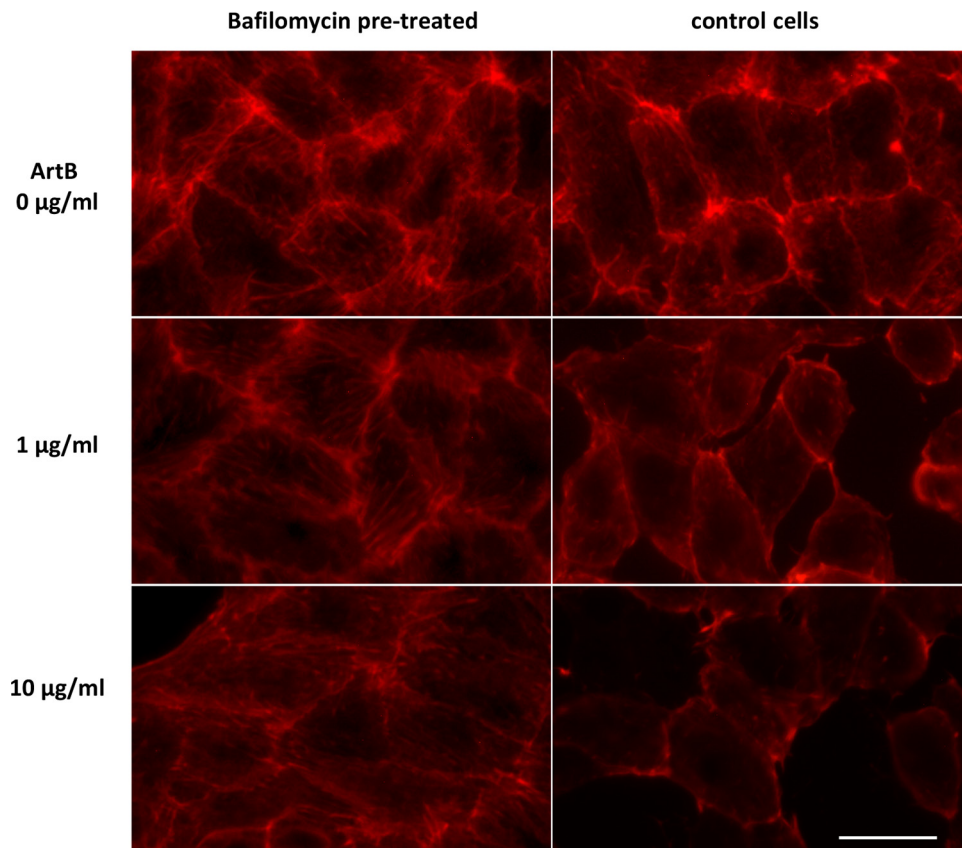
FIG 11 Effect of bafilomycin A1 on ArtB-induced cytoskeletal disorganization. Vero cells were pretreated with bafilomycin A1 (10 nM) for 1 h or left untreated (control cells) and then incubated with ArtB (0, 1, or 10 μg/ml) for 4 h, after which cells were fixed and permeabilized, F-actin was stained with 5 U/ml Alexa Flour 594-phalloidin, and cells were then examined by using an EVOS-fl high-resolution digital inverted fluorescence microscope. Bar, 25 μm.

are generated by these toxins differ from that of ArtB, which lacks enzymatic activity in its own right and does not form transmembrane pores. Vacuolating activity has also been reported for SubB, the B subunit of subtilase cytotoxin (31). Like ArtB and all the other toxins referred to above, SubB-induced vacuolation was inhibited by bafilomycin A1, indicating a requirement for V-ATPase, but further characterization has not been undertaken. SubB is 51% identical to ArtB, but whether the vacuolation property contributes to the pathogenicity of SubAB-producing *E. coli* strains is uncertain. The SubAB holotoxin is lethal for a wide variety of cell types at concentrations many orders of magnitude lower than that required to induce vacuolation. The situation with ArtB is quite different, as the ArtAB holotoxin lacks demonstrable A subunit-dependent cytotoxicity.

At present, the role of ArtAB in the pathogenesis of salmonellosis remains obscure, apart from its role as a delivery vehicle for CdtB in *S.* Typhi (10). However, in addition to the vacuolation phenotype reported in this study, we have shown that similar concentrations of ArtB trigger the secretion of chemokines, proinflammatory cytokines, and adhesion molecules in diverse cell types (12). Thus, ArtB may also contribute to pathogenesis independently of the A subunit by promoting and maintaining a strong inflammatory response at the site of infection as well as by inducing vacuolation. These findings may also have significance for infections caused by *Yersinia* spp., whose genomes encode homologues of ArtB but lack a cotranscribed cognate catalytic subunit.

MATERIALS AND METHODS

Purification of ArtB and ArtAB. Genes encoding ArtB and the ArtAB holotoxin with His$_6$ tags at the ArtB C terminus were cloned into pBAD18 (32), as previously described (12), and then transformed into an *E. coli* BL21(DE3) *lpxM*-negative mutant (33), which produces a penta-acylated lipopolysaccharide that has very low endotoxic activity. Proteins were expressed and purified by

using Ni-nitrilotriacetic acid (NTA) chromatography, as previously described (12). Where required, proteins were fluorescently labeled by using a DyLight 488 antibody labeling kit (Thermo Scientific) according to the manufacturer's instructions.

Cell culture. Vero (African Green Monkey kidney) cells were grown in Dulbecco's modified Eagle's medium (DMEM), CHO (Chinese hamster ovary) cells were grown in Ham's F-12 medium, HBMECs were grown in a 1:1 mixture of RPMI 1640 medium (catalogue number 11875; Gibco) and F-12 nutrient mixture (catalogue number 11765; Gibco), and U937 (human monocyte) cells were grown in RPMI 1640 medium. All media were supplemented with a solution containing 10 mM HEPES, 2 mM L-glutamine, 1 mM sodium pyruvate, 10% heat-inactivated fetal calf serum (FCS), 50 IU/ml penicillin, and 50 μg/ml streptomycin; all cells were incubated at 37°C in 5% CO_2.

Flow cytometry. Cells were incubated for 60 min with or without 10 μg/ml ArtB labeled with DyLight 488 at 4°C and then washed and analyzed immediately on a FACScan flow cytometer.

Neutral Red uptake assay. Vero cells were seeded into 24-well trays at a density of approximately 4×10^4 cells per well and incubated overnight at 37°C in 5% CO_2. Cell monolayers were preincubated with or without various inhibitors for 1 h and then pulsed with 10 μg/ml ArtB for 30 min, washed twice with PBS, and incubated in fresh medium for another 3.5 h. The medium was then removed, and cells were incubated for 1 h in fresh medium with 400 μg/ml Neutral Red (MP Biomedicals). Cells were washed twice with PBS and then agitated in 300 μl 50% ethanol–1% acetic acid for 10 min, after which 200-μl volumes were transferred into 96-well-flat bottom trays and the absorbance at 540 nm was measured by using a SpectraMax M2 microplate reader (Molecular Devices).

K^+ depletion. For the depletion of K^+, cell monolayers were washed twice with K buffer comprising 140 mM NaCl, 1 mM $CaCl_2$, 20 mM HEPES (pH 7.4), 1 mM $MgCl_2$, and 1 mg/ml glucose. Hypotonic buffer (K buffer diluted 1:1 with water) was then added, and cells were incubated for 5 min. Cells were washed again with K buffer three times and then incubated in the same buffer for 20 min. Cells were then treated with ArtB and assayed for Neutral Red uptake as described above. Control cells were similarly treated except that K buffer was supplemented with 10 mM KCl.

Inhibitors, subcellular markers, and antibodies. Chlorpromazine, MDC, bafilomycin A1, dynasore, nystatin, genistein, nocodazole, and brefeldin A were obtained from Sigma. The neuraminidase NanA from *Streptococcus pneumoniae* was purified as an N-terminally His$_6$-tagged fusion protein from recombinant *E. coli* M15 expressing the *nanA* gene cloned into the expression vector pQE30 (Qiagen) by Ni-NTA chromatography. Monoclonal antibody to His$_6$ (GenScript THE anti-His) was obtained from GenScript. ER-Tracker Red, wheat germ agglutinin-Texas Red (WGA-TR), and Alexa Fluor 594-phalloidin (obtained from Life Technologies) were used to label the endoplasmic reticulum, the Golgi apparatus/*trans*-Golgi network, and F-actin, respectively. Antibodies to Rab5 (C8B1), Rab7 (D95F2), Rab9 (D52G8), and EEA-1 were obtained from Cell Signaling, and antibody to golgin 97 was obtained from Abcam/Sapphire Bioscience. Alexa Fluor 488-conjugated goat anti-mouse IgG(H+L) and Alexa Fluor 594-conjugated goat anti-rabbit IgG(H+L) were obtained from Life Technologies.

Immunofluorescence and confocal microscopy. Vero cells were seeded onto 8-chamber glass microscope slides (Lab-Tek; Thermo Scientific) at a density of 2×10^4 cells per chamber and incubated overnight. Cell monolayers were then pulsed with 10 μg/ml ArtB for 30 min, washed twice with PBS, and replaced with fresh medium for the remainder of the incubation period. Cells were then washed with PBS and fixed with 4% paraformaldehyde in PBS for 20 min at room temperature (RT). Slides were then washed with PBS; permeabilized with 0.1% Triton X-100 in PBS for 5 min; washed with PBS; and blocked with a solution containing PBS, 10% FCS, and 2% normal goat serum for 1 h at RT. Slides were then incubated with primary antibody overnight at 4°C, washed with PBS, incubated with secondary antibody for 45 min at RT, washed thoroughly with PBS, and rinsed twice in deionized water. The chamber slide gasket was then removed, slides were air dried and then mounted in Vecta Shield mounting medium containing 4',6-diamidino-2-phenylindole (DAPI) (Vector Laboratories), and the coverslips were sealed with nail varnish. For F-actin staining, cells were permeabilized and then incubated with Alexa Fluor 594-phalloidin for 30 min, followed by washing and mounting as described above.

For cells incubated with ER-Tracker Red, after fixation, cells were permeabilized with 0.5% saponin in PBS for 10 min; washed with PBS–0.1% saponin; and then blocked with a solution containing PBS, 10% FCS, 2% normal goat serum, and 0.1% saponin for 1 h at RT. Cells were incubated with primary antibody overnight at 4°C in PBS–0.1% saponin, washed with PBS–0.1% saponin, incubated with secondary antibody for 45 min at RT in PBS–0.1% saponin, washed thoroughly with PBS, incubated with DAPI (500 ng/ml) in PBS for 5 min at RT, washed thoroughly with PBS, and rinsed twice with deionized water. The chamber slide gasket was then removed, and slides were air dried; slides were then mounted in 80% glycerol. For WGA-TR staining, after fixation, cells were incubated with WGA-TR for 20 min, washed with PBS, and then stained as described above for ER-Tracker Red.

Fluorescence images were obtained by using a Leica SP5 spectral scanning confocal microscope (Leica Microsystems) with a 63× (1.40-numerical-aperture [NA]) oil immersion objective lens. Confocal settings used for image capture were held constant in comparison experiments. Images were processed, and colocalization was quantified by using ImageJ software and the JACoP plug-in. The colocalization values obtained represent Manders' M1 overlap coefficient. This value calculates the proportion of ArtB-stained pixels that colocalize with pixels stained by the second antibody/marker. Background fluorescence was subtracted by using regions of the cell devoid of staining. For Rab5, Rab7, Rab9, and EEA-1, colocalization was calculated by using the whole cell field. For ER colocalization, comparisons of regions positive for ER-Tracker Red were selected and used as a constant. Data were processed and analyzed statistically by using unpaired *t* tests in GraphPad Prism.

ACKNOWLEDGMENTS

REFERENCES

1. Beddoe T, Paton AW, Le Nours J, Rossjohn J, Paton JC. 2010. Structure, biological functions and applications of the AB$_5$ toxins. Trends Biochem Sci 35:411–418. https://doi.org/10.1016/j.tibs.2010.02.003.

2. Paton AW, Srimanote P, Talbot UM, Wang H, Paton JC. 2004. A new family of potent AB5 cytotoxins produced by Shiga toxigenic *Escherichia coli*. J Exp Med 200:35–46. https://doi.org/10.1084/jem.20040392.

3. Paton AW, Beddoe T, Thorpe CM, Whisstock JC, Wilce MC, Rossjohn J, Talbot UM, Paton JC. 2006. AB5 subtilase cytotoxin inactivates the endoplasmic reticulum chaperone BiP. Nature 443:548–552. https://doi.org/10.1038/nature05124.

4. Wolfson JJ, May KL, Thorpe CM, Jandhyala DM, Paton JC, Paton AW. 2008. Subtilase cytotoxin activates PERK, IRE1 and ATF6 endoplasmic reticulum stress-signalling pathways. Cell Microbiol 10:1775–1786. https://doi.org/10.1111/j.1462-5822.2008.01164.x.

5. May KL, Paton JC, Paton AW. 2010. *Escherichia coli* subtilase cytotoxin induces apoptosis regulated by host Bcl-2 family proteins, Bax/Bak. Infect Immun 78:4691–4696. https://doi.org/10.1128/IAI.00801-10.

6. Yahiro K, Morinaga N, Moss J, Noda M. 2010. Subtilase cytotoxin induces apoptosis in HeLa cells by mitochondrial permeabilization via activation of Bax/Bak, independent of C/EBF-homologue protein (CHOP), Ire1alpha or JNK signaling. Microb Pathog 49:153–163. https://doi.org/10.1016/j.micpath.2010.05.007.

7. Byres E, Paton AW, Paton JC, Löfling JC, Smith DF, Wilce MCJ, Talbot UM, Chong DC, Yu H, Huang S, Chen X, Varki NM, Varki A, Rossjohn J, Beddoe T. 2008. Incorporation of a non-human glycan mediates human susceptibility to a bacterial toxin. Nature 456:648–652. https://doi.org/10.1038/nature07428.

8. Saitoh M, Tanaka K, Nishimori K, Makino S, Kanno T, Ishihara R, Hatama S, Kitano R, Kishima M, Sameshima T, Akiba M, Nakazawa M, Yokomizo Y, Uchida I. 2005. The *artAB* genes encode a putative ADP-ribosyltransferase toxin homologue associated with *Salmonella enterica* serovar Typhimurium DT104. Microbiology 151:3089–3096. https://doi.org/10.1099/mic.0.27933-0.

9. Uchida I, Ishihara R, Tanaka K, Hata E, Makino S, Kanno T, Hatama S, Kishima M, Akiba M, Watanabe A, Kubota T. 2009. *Salmonella enterica* serotype Typhimurium DT104 ArtA-dependent modification of pertussis toxin-sensitive G proteins in the presence of [^{32}P]NAD. Microbiology 155:3710–3718. https://doi.org/10.1099/mic.0.028399-0.

10. Spanò S, Ugalde JE, Galán JE. 2008. Delivery of a *Salmonella* Typhi exotoxin from a host intracellular compartment. Cell Host Microbe 3:30–38. https://doi.org/10.1016/j.chom.2007.11.001.

11. Song J, Gao X, Galán JE. 2013. Structure and function of the *Salmonella* Typhi chimaeric A(2)B(5) typhoid toxin. Nature 499:350–354. https://doi.org/10.1038/nature12377.

12. Wang H, Paton JC, Herdman BP, Rogers TJ, Beddoe T, Paton AW. 2013. The B subunit of an AB5 toxin produced by *Salmonella enterica* serovar Typhi up-regulates chemokines, cytokines, and adhesion molecules in human macrophage, colonic epithelial, and brain microvascular endothelial cell lines. Infect Immun 81:673–683. https://doi.org/10.1128/IAI.01043-12.

13. Larkin JM, Donzell WC, Anderson RG. 1986. Potassium-dependent assembly of coated pits: new coated pits form as planar clathrin lattices. J Cell Biol 103:2619–2627. https://doi.org/10.1083/jcb.103.6.2619.

14. Ivanov AI. 2008. Pharmacological inhibitions of endocytic pathways: is it specific enough to be useful?, p 15–33. *In* Ivanov AI (ed), Methods in molecular biology, vol 440. Exocytosis and endocytosis. Humana Press, Totowa, NJ.

15. Wang LH, Rothberg KG, Anderson RG. 1993. Mis-assembly of clathrin lattices on endosomes reveals a regulatory switch for coated pit formation. J Cell Biol 123:1107–1117. https://doi.org/10.1083/jcb.123.5.1107.

16. Yoshimori T, Yamamoto A, Moriyama Y, Futai M, Tashiro Y. 1991. Bafilomycin A1, a specific inhibitor of vacuolar-type H+-ATPase, inhibits acidification and protein degradation in lysosomes of cultured cells. J Biol Chem 266:17707–17712.

17. Parton RG, Joggerst B, Simons K. 1994. Regulated internalization of caveolae. J Cell Biol 127:1199–1215. https://doi.org/10.1083/jcb.127.5.1199.

18. Nabi IR, Le PU. 2003. Caveolae/raft-dependent endocytosis. J Cell Biol 161:673–677. https://doi.org/10.1083/jcb.200302028.

19. Singh RD, Puri V, Valiyaveettil JT, Marks DL, Bittman R, Pagano RE. 2003. Selective caveolin-1-dependent endocytosis of glycosphingolipids. Mol Biol Cell 14:3254–3265. https://doi.org/10.1091/mbc.E02-12-0809.

20. Olkkonen V, Stenmark H. 1997. Role of Rab GTPases in membrane traffic. Int Rev Cytol 176:1–85. https://doi.org/10.1016/S0074-7696(08)61608-3.

21. Wilson JM, de Hoop M, Zorzi N, Toh BH, Dotti CG, Parton RG. 2000. EEA1, a tethering protein of the early sorting endosome, shows a polarized distribution in hippocampal neurons, epithelial cells, and fibroblasts. Mol Biol Cell 11:2657–2671. https://doi.org/10.1091/mbc.11.8.2657.

22. Barbero P, Bittova L, Pfeffer SR. 2002. Visualization of Rab9-mediated vesicle transport from endosomes to the trans-Golgi in living cells. J Cell Biol 156:511–518. https://doi.org/10.1083/jcb.200109030.

23. Stenmark H. 2009. Rab GTPases as coordinators of vesicle traffic. Nat Rev Mol Cell Biol 10:513–525. https://doi.org/10.1038/nrm2728.

24. Chong DC, Paton JC, Thorpe CM, Paton AW. 2008. Clathrin-dependent trafficking of subtilase cytotoxin, a novel AB$_5$ toxin that targets the ER chaperone BiP. Cell Microbiol 10:795–806. https://doi.org/10.1111/j.1462-5822.2007.01085.x.

25. Deng L, Song J, Gao X, Wang J, Yu H, Chen X, Varki N, Naito-Matsui Y, Galán JE, Varki A. 2014. Host adaptation of a bacterial toxin from the human pathogen *Salmonella* Typhi. Cell 159:1290–1299. https://doi.org/10.1016/j.cell.2014.10.057.

26. Boquet P, Ricci V. 2012. Intoxication strategy of *Helicobacter pylori* VacA toxin. Trends Microbiol 20:165–174. https://doi.org/10.1016/j.tim.2012.01.008.

27. Nagahama M, Itohayashi Y, Hara H, Higashihara M, Fukatani Y, Takagishi T, Oda M, Kobayashi K, Nakagawa I, Sakurai J. 2011. Cellular vacuolation induced by *Clostridium perfringens* epsilon-toxin. FEBS J 278:3395–3407. https://doi.org/10.1111/j.1742-4658.2011.08263.x.

28. Johnson C, Kannan TR, Baseman JB. 2011. Cellular vacuoles induced by *Mycoplasma pneumoniae* CARDS toxin originate from Rab9-associated compartments. PLoS One 6:e22877. https://doi.org/10.1371/journal.pone.0022877.

29. Kannan TR, Baseman JB. 2006. ADP-ribosylating and vacuolating cytotoxin of *Mycoplasma pneumoniae* represents unique virulence determinant among bacterial pathogens. Proc Natl Acad Sci U S A 103:6724–6729. https://doi.org/10.1073/pnas.0510644103.

30. Krishnan M, Kannan TR, Baseman JB. 2013. *Mycoplasma pneumoniae* CARDS toxin is internalized via clathrin-mediated endocytosis. PLoS One 8:e62706. https://doi.org/10.1371/journal.pone.0062706.

31. Morinaga N, Yahiro K, Matsuura G, Watanabe M, Nomura F, Moss J, Noda M. 2007. Two distinct cytotoxic activities of subtilase cytotoxin produced by Shiga-toxigenic *Escherichia coli*. Infect Immun 75:488–496. https://doi.org/10.1128/IAI.01336-06.

32. Guzman LM, Belin D, Carson MJ, Beckwith J. 1995. Tight regulation, modulation, and high-level expression by vectors containing the arabinose pBAD promoter. J Bacteriol 177:4121–4130. https://doi.org/10.1128/jb.177.14.4121-4130.1995.

33. Cognet I, de Coignac AB, Magistrelli G, Jeannin P, Aubry JP, Maisnier-Patin K, Caron G, Chevalier S, Humbert F, Nguyen T, Beck A, Velin D, Delneste Y, Malissard M, Gauchat JF. 2003. Expression of recombinant proteins in a lipid A mutant of *Escherichia coli* BL21 with a strongly reduced capacity to induce dendritic cell activation and maturation. J Immunol Methods 272:199–210. https://doi.org/10.1016/S0022-1759(02)00506-9.